Binary Thermal Encoding by Energy Shielding and Harvesting Units

Run Hu,* Shiyao Huang, Meng Wang, Liliang Zhou, Xiayao Peng, and Xiaobing Luo†
School of Energy and Power Engineering, Huazhong University of Science and Technology, Wuhan 430074, China

(Received 31 August 2018; revised manuscript received 20 October 2018; published 14 November 2018)

Optical and thermal metamaterials-based devices have been extensively explored under the guidance of transformation optics/thermotics theories to tune light and heat propagation to realize unprecedented functions, such as cloaking, concentrating, camouflaging, etc. Other than these functions, what else can they do? In this paper, we demonstrate another interesting and potential application, thermal encoding, based on the thermal energy shielding and harvesting units. The proposed thermal encoding protocol takes advantage of the binary (contrary) states of heat flux through two units, which can be encoded as binary digits of 1 and 0, respectively. Steady and transient simulations and experiments validate the feasibility of thermal encoding, which can be further effectively encrypted depending on the encoding or decoding protocol. Such thermal encoding supplements the existing implementations of thermal memory or computing. The proposed encoding protocol may open an alternative avenue for triggering counterpart developments by utilizing the binary states of electromagnetic and optical metamaterials for information encoding, decoding, and storage.

DOI: 10.1103/PhysRevApplied.10.054032

I. INTRODUCTION

As the quintessential demonstration of transformation optics (TO) theory, the invisible optical cloak, which can render an object invisible, has opened a nearly borderless space for thought with a series of successful counterpart extensions in electromagnetics, thermotics, acoustics, and mechanics fields [1–5]. The essence of TO theory lies in the form invariance of the governing equations under coordinate transformation from one space to another, while giving rise to stringent requirements of transformed material parameters with anisotropy, inhomogeneity, and singularity. The naturally existing materials usually fail to meet such severe requirements and the alternative artificial manmade materials, metamaterials, have been widely used in the recent decade to make the implementation of such *ad hoc* cloaks possible. Compared with electromagnetic waves, heat does not possess phase information and the counterpart thermal cloak and transformation thermotics seem more likely to successfully achieve heat flow manipulation with many derivative functions, such as thermal cloaking [6–9], concentrating [8,10–12], rotating [8,13], refracting [14], reflecting [15], and camouflaging [16,17] with validation in theory or in experiments. In particular, a thermal cloak can tune the heat flux of an invisible region and return it to its original direction without disturbing the heat flux lines and isotherms outside, which then looks as though there is no object inside. Such a cloaking structure can be used to passively shield thermal energy from certain regions, thus it is called an energy shielding unit (ESU). On the contrary, a thermal concentrator can attract heat into a central region and result in a considerably large temperature gradient there and realize energy harvesting, thus it is called an energy harvesting unit (EHU). The main difference is the heat flux in the central region of these two structures, i.e., one is nearly zero and the other is very large. Two such contrary functions based on ESU and EHU significantly change the heat flow at certain regions and can even be switched [18]. So far, the ESU and EHU are only used to tune heat flow, but what else can they be used for?

Information storage involves alternative state variables and has most often been realized in electronic memory. Information is stored by placing or removing electrons on a capacitor-transistor network. The presence and absence of electrons changes the behaviors of the transistor, which is then interpreted as a binary data bit (1 or 0) [19]. Encouraged by the success and wide application of electronic memory, alternatives are being explored, such as magnetic memory [20], phase-change memory [19,21–23], thermal memory [24–27], etc. In magnetic memory, information is written to and read from the storage medium as it moves past the read-and-write head that operates very close (approximately 10 nm) to the magnetic surface. The read-and-write head can detect and modify the magnetization of the storage medium with Boolean magnetic polarities as 1 and 0. In phase-change memory, the chalcogenide alloy [such as $Ge_2Sb_2Te_5$, (GST)] can be tuned

*hurun@hust.edu.cn
†luoxb@hust.edu.cn

to change phases from an amorphous state to a crystallization state by heating or cooling. The crystalline and amorphous states of chalcogenide alloy have dramatically different electrical resistivity values, thus the amorphous high-resistance state represents a binary 0, while the crystalline low-resistance state represents a binary 1. As for thermal memory, Li *et al.* [25] proposed a theoretical thermal memory by replacing the electric voltages and currents with thermostats at fixed temperatures by controlling phonon transport in molecular dynamics for information storage. In experiments, Xie *et al.* [26] employed a metal-insulator transition of a VO_2 crystal to store and retain thermal information with two temperature states as input T_{in} and output T_{out}, which serve as the logical Boolean units of 1 (T_{in}) and 0 (T_{out}) for writing and reading. In essence, this is also a kind of phase-change memory that uses a metal-insulator phase change. All these memory technologies use binary states to denote the digital bits of 1 and 0, such as the presence/absence of electrons, binary magnetic polarities, high/low resistances of a chalcogenide alloy, and high/low temperatures.

Inspired by the contrary characteristics of ESU and EHU and the requirements for thermal memory, we propose a different kind of thermal memory scheme by encoding the heat flux in the central regions of ESU and EHU to represent the binary states as 1 and 0 in this paper. Details of the encoding and performance evaluation process of these two basic units are presented in one and two dimensions, with implications of successful extensions to three dimensions as well. Transient measurement is conducted to reveal that the proposed ESU and EHU can also be effectively encoded in a nonequilibrium system. Experiments reveal that such a thermal encoding can be further encrypted depending on the preset critical-heat flux, which increases the memory density. Such a thermal memory scheme extends the application extension of state-of-the-art thermal metamaterials and supplements the implementations of existing thermal memory or computing.

II. TRANSFORMATION THERMOTICS

Heat conduction without a heat source is governed by Fourier's law as $\rho c(\partial T/\partial t) = \nabla \cdot (\kappa \nabla T)$, where ρ and c are the density and thermal capacity, respectively, $\boldsymbol{\kappa}$ is the thermal conductivity tensor, and T is the temperature. According to the principle of transformation thermotics, the Fourier equation maintains its form after coordinate transformation, i.e., $\rho' c'(\partial T'/\partial t) = \nabla' \cdot (\kappa' \nabla T')$. The transformed thermal conductivity tensor from the virtual space (x, y, z) to the real space (x', y', z') can be expressed as [1,7,16]

$$\kappa' = \begin{bmatrix} \kappa'_{xx} & \kappa'_{xy} & \kappa'_{xz} \\ \kappa'_{yx} & \kappa'_{yy} & \kappa'_{yz} \\ \kappa'_{zx} & \kappa'_{zy} & \kappa'_{zz} \end{bmatrix} = \frac{\mathbf{J}\kappa_0\mathbf{J}^{\mathrm{T}}}{\det(\mathbf{J})}, \qquad (1)$$

where κ_0 is the homogeneous thermal conductivity in the virtual space, $\mathbf{J}$ is the Jacobian matrix of the two spaces, and $\mathbf{J}^{\mathrm{T}}$ is the transposition of $\mathbf{J}$. To realize thermal cloaking, one can compress a circular region ($r \le b$) in the virtual space into an annular region ($a \le r' \le b$) in the real space by following cylindrical coordinate transformation as $\{r' = (b-a)r/b + a,\ \theta' = \theta,\ z' = z\}$, where a and b are the inner and outer radii of the annular region. Substituting into Eq. (1), we can obtain the transformed thermal properties of an ideal thermal cloak as $\kappa' = \kappa_0 \mathrm{diag}(\kappa'_r, \kappa'_\theta, 1) = \kappa_0 \mathrm{diag}[(r'-a)/r', r'/(r'-a), 1]$ and $\rho' c' = [(r'-a)/r'][a/(b-a)]^2 \rho c$ [7]. With the transformed $\boldsymbol{\kappa}'$ and $\rho' c'$, we can obtain the temperature profile of an ideal thermal cloak, as shown in Fig. 1(a). It is seen that both the heat flow lines and the isotherms are "tuned" to pass around the central region perfectly without distorting the horizontal heat flow lines and the orthogonal isotherms outside the annular region. It is thus shown that any object inside the central region will be shielded from the outside heat source, therefore, we call it ESU here after. The fundamental reason for such a cloaking effect can be attributed to the singularity of the tangential component of $\boldsymbol{\kappa}'$ $[r'/(r'-a)]$ when r' approaches a. When changing $\boldsymbol{\kappa}'$ from $\kappa' = \kappa_0 \mathrm{diag}(\kappa'_r, \kappa'_\theta, 1)$ to $\kappa' = \kappa_0 \mathrm{diag}(\kappa'_\theta, \kappa'_r, 1)$, we can realize the thermal concentrator as shown in Fig. 1(b). It is seen that heat will be concentrated/attracted into the central region, resulting in a considerably larger temperature gradient there. Such thermal concentrator structures can be used to harvest low-grade thermal energy and realize local heating [10], thus we call it EHU here after. Though the required $\boldsymbol{\kappa}'$ is anisotropic, inhomogeneous, and even has singularity, we can realize the equivalent cloaking/concentrating effect using layered homogenous materials. When only two isotropic materials A and B with thermal conductivity κ_A and κ_B are employed, the transformed $\boldsymbol{\kappa}'$ can be realized based on effective medium theory (EMT) by alternatively stacking the uniformly thick materials A and B with $\kappa_{A,B} = \kappa'_\theta \pm \sqrt{\kappa'^2_\theta - \kappa'_r \kappa'_\theta}$ for ESU and $\kappa_{A,B} = \kappa'_r \pm \sqrt{\kappa'^2_r - \kappa'_r \kappa'_\theta}$ for EHU, respectively. For instance, with concentric thin-layer materials such as epoxy [$\kappa_{\text{epoxy}} = 7.78\ \mathrm{W/(m\,K)}$] and natural latex rubber [$\kappa_{\text{rubber}} = 0.13\ \mathrm{W/(m\,K)}$], an ESU can be fabricated and realized [6]; with sensu-shape thin-layer materials such as copper [$\kappa_{\text{copper}} = 398\ \mathrm{W/(m\,K)}$] and polydimethylsiloxane (PDMS, [$\kappa_{\text{PDMS}} = 0.16\ \mathrm{W/(m\,K)}$]), an EHU can be fabricated and realized [9,10]. Further, we may discover that the radial and tangential components of the transformed $\boldsymbol{\kappa}'$ are reciprocal to each other, thus we can define the radial component as $1/C$ and the tangential component as C where C is a constant for realizing the approximate effects of ESU and EHU with natural existing materials without singularity. For an ESU, the radial component is less than the tangential one, thus C is much larger than 1 and belongs to $[b/(b-a), \infty)$; for EHU, C is less than 1 and belongs

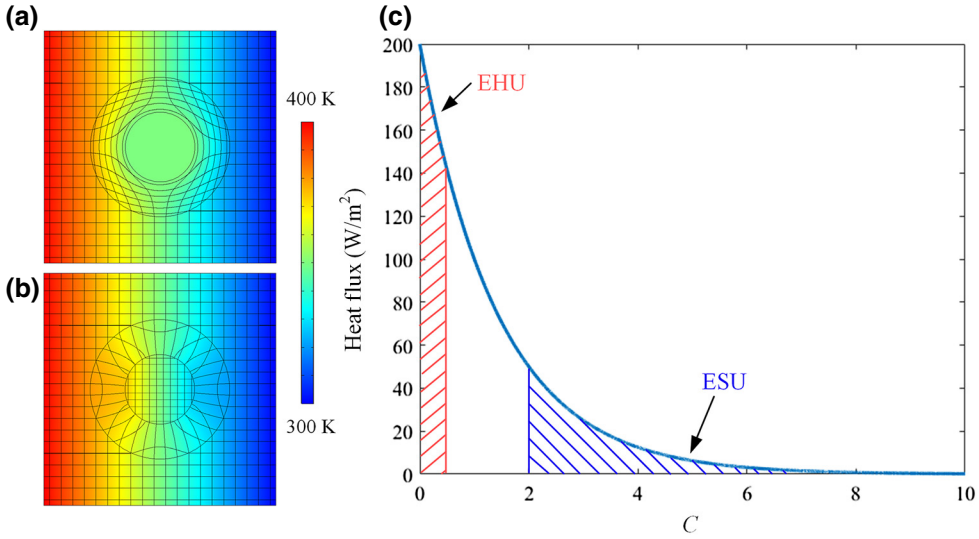

FIG. 1. Temperature profile with heat flux lines and isotherms for (a) ESU and (b) EHU. Heat moves from the left boundary (400 K) to the right boundary (300 K) without consideration of heat convection. The central region and the outside region are PDMS with $\kappa_{\mathrm{PDMS}} = 0.16\,\mathrm{W/(m\,K)}$, $\rho = 970\,\mathrm{kg/m^3}$, and $c = 1460\,\mathrm{J/(kg\,K)}$. The thermal properties of the annular region are according to the calculations. The radii of the annular regions are 15 mm and 30 mm. The dimensions of the whole plane $100 \times 100\,\mathrm{mm^2}$. (c) Heat flux along the x direction in the central region with varying C. Red and blue shadow regions denote the upper and lower bounds of heat flux for EHU and ESU, respectively.

to $[0, (b-a)/b]$. It is believed that although the ESU and EHU effects realized by homogenous materials with a constant thermal conductivity of C may be not as perfect as those realized by transformed inhomogeneous $\boldsymbol{\kappa}'$, the ESU and EHU performances will be improved by achieving very large/small C values, respectively.

A. Theoretical analysis

To explore the physical understanding of ESU and EHU with homogenous materials, we apply a rigorous mathematical model for comparison analyses. The steady heat conduction equation in a cylindrical coordinate is

$$\frac{\partial^2 T}{\partial r^2} + \frac{1}{r}\cdot\frac{\partial T}{\partial r} + \frac{\varepsilon^2}{r^2}\cdot\frac{\partial^2 T}{\partial \theta^2} = 0\,, \tag{2}$$

where $\varepsilon = 1$ for the central region $[r \in (0, a]]$ and outside region $[r \in [b, \infty)]$, and $\varepsilon = C$ for the annular region $[r \in (a, b)]$. The solutions of Eq. (2) in different regions can be generally expressed as [6]

$$T_i = \sum_{n=1}^{\infty} [A^i_{2n-1} r^{(2n-1)\varepsilon} + B^i_{2n-1} r^{-(2n-1)\varepsilon}] \cos(2n-1)\theta, \tag{3}$$

where i (=1,2,3) denote the central, annular, and outside regions, respectively, A^i_{2n-1} and B^i_{2n-1} are the constants to be determined by the boundary conditions, and T_i denotes the temperature in different regions. A temperature distribution with a uniform temperature gradient $-(T_0/x_0)$ is externally applied in the x direction. Though the boundary conditions may change for different application situations, a uniform outside temperature gradient can be assumed here as a constant for simplification, and the boundary conditions can be considered by assigning the varying T_0/x_0. Since T_3 tends to be proportional to $r\cos\theta$, we only need to consider $n = 1$ with $A^3_1 = -(T_0/x_0)$ and $B^3_1 = 0$. Since T_1 is bounded when $r \to 0$, B^1_1 should decrease to 0. Considering the temperature continuity and radial-heat-flux continuity across the interfaces $r = a$ and $r = b$, and assuming the central region and outside region are κ_1 and κ_3, we can obtain

$$\begin{bmatrix} 1 & -a^{\varepsilon-1} & -a^{-\varepsilon-1} & 0 \\ \kappa_1 & -a^{\varepsilon-1} & a^{-\varepsilon-1} & 0 \\ 0 & b^{\varepsilon-1} & b^{-\varepsilon-1} & -1 \\ 0 & b^{\varepsilon-1} & -b^{-\varepsilon-1} & -\kappa_3 \end{bmatrix} \begin{bmatrix} A^1_1 \\ A^2_1 \\ B^2_1 \\ A^3_1 \end{bmatrix} = 0. \tag{4}$$

Solving Eq. (4) and assuming $\kappa_1 = \kappa_3 = 1\,\mathrm{W/(m\,K)}$, we obtain the following temperature profiles as $T_1 = -(T_0/x_0)(a/b)^{\varepsilon-1} r\cos\theta$, $T_2 = -(T_0/x_0)(r/b)^{\varepsilon-1} r\cos\theta$, and $T_3 = -(T_0/x_0)\, r\cos\theta$. We can see that when $\varepsilon = 1$, $T_1 = T_2 = T_3$, corresponding to free space. Focusing on the heat flux in the central region along the x direction, we obtain

$$q_x = -\kappa_1 \frac{\partial T_1}{\partial x} = \frac{T_0}{x_0}\left(\frac{a}{b}\right)^{\varepsilon-1}. \tag{5}$$

For ESU, $\varepsilon = C \in [b/(b-a), \infty)$, then $q_x \in (0, T_0/x_0\,(a/b)^{a/(b-a)}]$. For EHU, $\varepsilon = C \in [0, (b-a)/b]$, then $q_x \in [(T_0/x_0)(a/b)^{-(a/b)}, (T_0/x_0)(b/a)]$. In other words, when

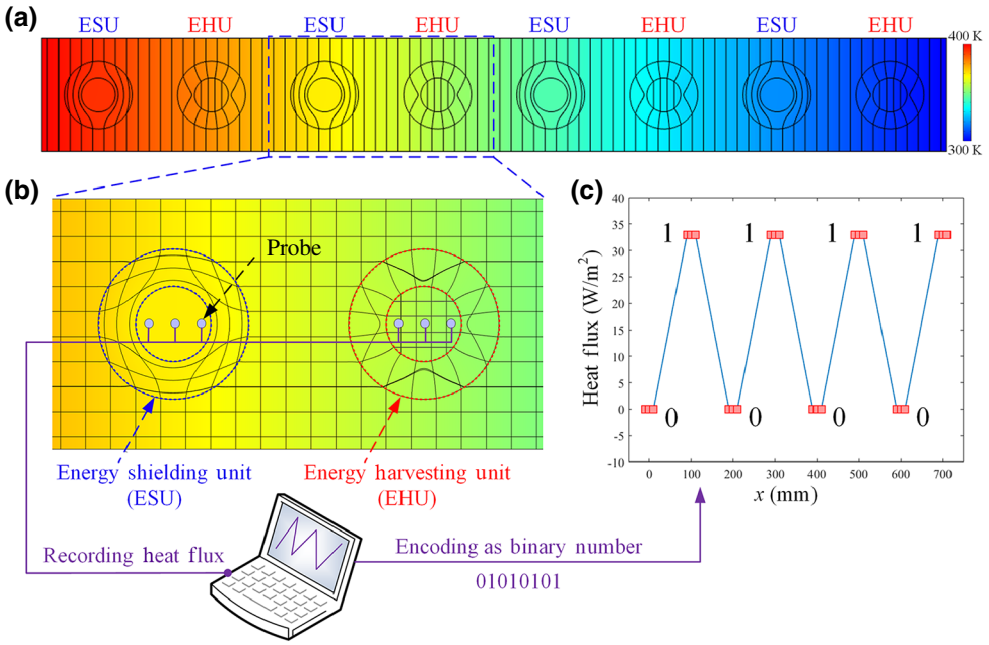

FIG. 2. One-dimensional thermal encoding based on a series of ESUs and EHUs. (a) Steady temperature profile and isotherms of ESUs and EHUs in series. The dimensions of the whole plane are 800×100 mm^2, while each ESU and EHU has the same dimensions as those in Fig. 1. All the other simulation conditions are the same. (b) Zoom-in temperature profiles of ESU and EHU with heat flux lines and isotherms. Thermal energy is observed to be shielded and harvested by the ESU and EHU, respectively. Three heat-flux probes are assembled in the central region of each ESU and EHU to detect the heat flux along the x direction. (c) Heat-flux curve detected by all the probes (a) along the x direction. The heat flux in all ESUs and EHUs are the same at two separated levels, enabling binary encoding based on the probed heat flux. Based on such an encoding protocol, the ESUs and EHUs in (a) can be encoded as the binary number 01010101.

C is large enough, $q_x \to 0$, which implies that nearly no thermal energy enters the central region, corresponding to the ESU effect. When C approaches 0, a relatively large amount of thermal energy enters the central region, corresponding to the EHU effect. The variation of q_x with C is plotted in Fig. 1(c). It is obvious that the heat flux in EHU is much larger than that in ESU with a large gap between the two units, especially for the extremely large C for ESU and extremely small $1/C$ for EHU.

III. RESULTS AND DISCUSSIONS

When arranging the ESU and EHU in series, as shown in Fig. 2(a), we can observe the same behaviors of isotherms and heat flux lines (not shown) for all the ESUs and EHUs, respectively. For all ESUs, the heat flux lines will be tuned around the central region, while for all EHUs, the heat flux lines will be concentrated in the central region, even when the two ESUs or EHUs are a long distance apart. This implies that although the temperature is decreasing from left to the right, the ESU and EHU effects are maintained along the heat flow. Such ESU and EHU effects can be observed more clearly in Fig. 2(b), which is almost the same as Fig. 1 except for the temperature value. Inspired by such ESU and EHU effects, we assemble three heat-flux probes in the central region along the x direction in all the ESU and EHU regions and record the heat-flux values. The probed heat flux is plotted in Fig. 2(c). It is seen that the heat flux in all ESU regions is stable at approximately 0.025 W/m^2, while the heat flux in all EHU regions is stable at approximately 32.974 W/m^2, even downstream from the low temperature. This implies that the probed heat flux is independent of the local temperature, but dependent on the structure on which the probes sit. Such a stable heat flux at two separated levels enables binary encoding: the nearly zero heat flux represents the binary digit of 0, while the large heat flux represents the binary digit of 1. Based on such an encoding protocol, the probed heat flux in Fig. 2 can be encoded as the binary number 01010101.

The transient heat conduction process is shown in Fig. 3(a). From the initial state to the steady state, heat gradually diffuses from the left to the right with the increasing temperature at the right end. In the initial state, the isotherms are much closer at the left end that those at the right end, implying a larger temperature gradient at the left end. With time, the isotherms progressively stretch to the right end, which implies a gradually uniform temperature gradient in the whole plane. When focusing on all the ESU and EHU regions, we can see that even at different temperatures at different states, the isotherm and heat flux lines

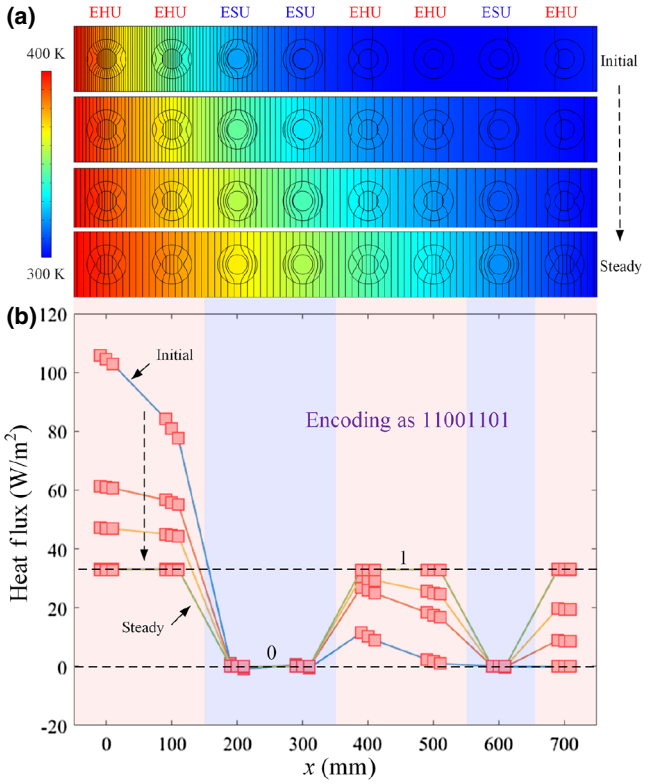

FIG. 3. (a) Transient temperature profiles with isotherms of ESUs and EHUs in series from the initial state to a steady state. All the simulation conditions are the same as those in Fig. 2 except for the sequence of the ESUs and EHUs layout. (b) Heat-flux evolution from the initial state to the steady state for all of the probes. The heat fluxes of all ESUs are stable at nearly zero over time, while the heat fluxes of all EHUs tend to be at the same level, enabling quick binary thermal encoding for a transient scheme. Based on such an encoding protocol, the ESUs and EHUs in (a) can be encoded as the binary number 11001101.

(not shown) are tuned to flow around or to concentrate in the central region. The only difference is the spatial density of the isotherms at different states. Similarly, the three heat-flux probes record the local heat flux along the x direction, which is plotted in Fig. 3(b). It is seen that with time, the heat flux in the central region of the EHU gradually changes to a steady value of approximately 32.97 W/m^2, while the heat flux in the central region of the ESU is almost the same at approximately 0.03 W/m^2. In particular, the heat flux upstream in the EHU decreases, while downstream it gradually increases, which corresponds to the stretching of isotherms from upstream to downstream with time. Such a large heat flux difference between the ESU and EHU regions represents obvious binary states and enables binary encoding: the nearly zero heat flux in the ESU region represents the binary digit of 0, while the large heat flux in the EHU region represents the binary digit of 1. These varying fluxes play the same role as the binary states in electronic, magnetic, and other thermal memory technologies. Moreover, we may find that without waiting for the steady state, the heat flux difference between the ESU and EHU regions is still obvious even at the beginning. Therefore, we may define a threshold value of heat flux such that when the heat flux is larger than the threshold, it may be interpreted as 1; when the heat flux is much smaller than the threshold, it may be interpreted as 0. Such a behavior enables thermal encoding with a transient scheme. Based on such an encoding protocol, the ESU and EHU regions in Fig. 3(a) can be encoded as the binary number 11001101. To further shorten the lagging of the thermal encoding, we may design the structure with smaller sizes and higher thermal diffusivity, or exactly define a proper threshold heat flux without waiting for a steady temperature field.

Further, the proposed ESU and EHU regions can not only be used for one-dimensional (1D) thermal encoding, but can also be used for two- and three-dimensional (2D and 3D) cases. Figure 4 shows the 2D case based on a 5×5 array of ESU and EHU regions. We also observe the same behaviors for the isotherms and heat flux lines (not shown) for all the ESU and EHU regions on the square plane in Fig. 4(a). The corresponding local heat flux in the inner cylinder array is plotted in Fig. 4(b), and the probed heat fluxes along the x direction and y direction are plotted in Fig. 4(c). From both Figs. 4(b) and 4(c), two clearly separated states of heat flux in the ESU and EHU regions are observed. With the same encoding protocol, all the ESU and EHU regions can be interpreted as an array of binary numbers, as shown in Fig. 4(d). The binary number array can be stored in a computer either along the column direction or along the row direction for information storage.

For further validating the proposed binary thermal encoding concept, we fabricate prototypes of ESU and EHU regions with copper, as shown in Figs. 5(a) and 5(b). In addition to two EHUs and three ESUs, three cylinders of the same sizes are also fabricated (called reference units here after). The ESUs are made of copper rings with a thickness of 2 mm and the EHUs are made of copper wheel-shaped structures with a central angle of 10°. The outer and inner radii of the ESUs and EHUs are 25 and 10 mm, respectively. All the units are mounted on a 380-mm-long, 160-mm-wide, and 10-mm-thick rectangular plate. The reference units and the rectangular plates are made of invar steel [$\kappa = 11$ W/(m K)]. All the surfaces are cooled with a natural convection coefficient of 2 W/(m^2 K). Two feet are retained for heating and cooling: the left one is maintained at 120 °C by an electric heater and the right one is maintained at room temperature, 25 °C, thus heat is conducted from the left to the right. In the experiment, after mounting all the units, the surfaces are wrapped with black tape to ensure that the emissivity is consistent. An IR camera (FLIR SC620) is used to observe the temperature fields and the emissivity is set as 0.98 with calibration by a

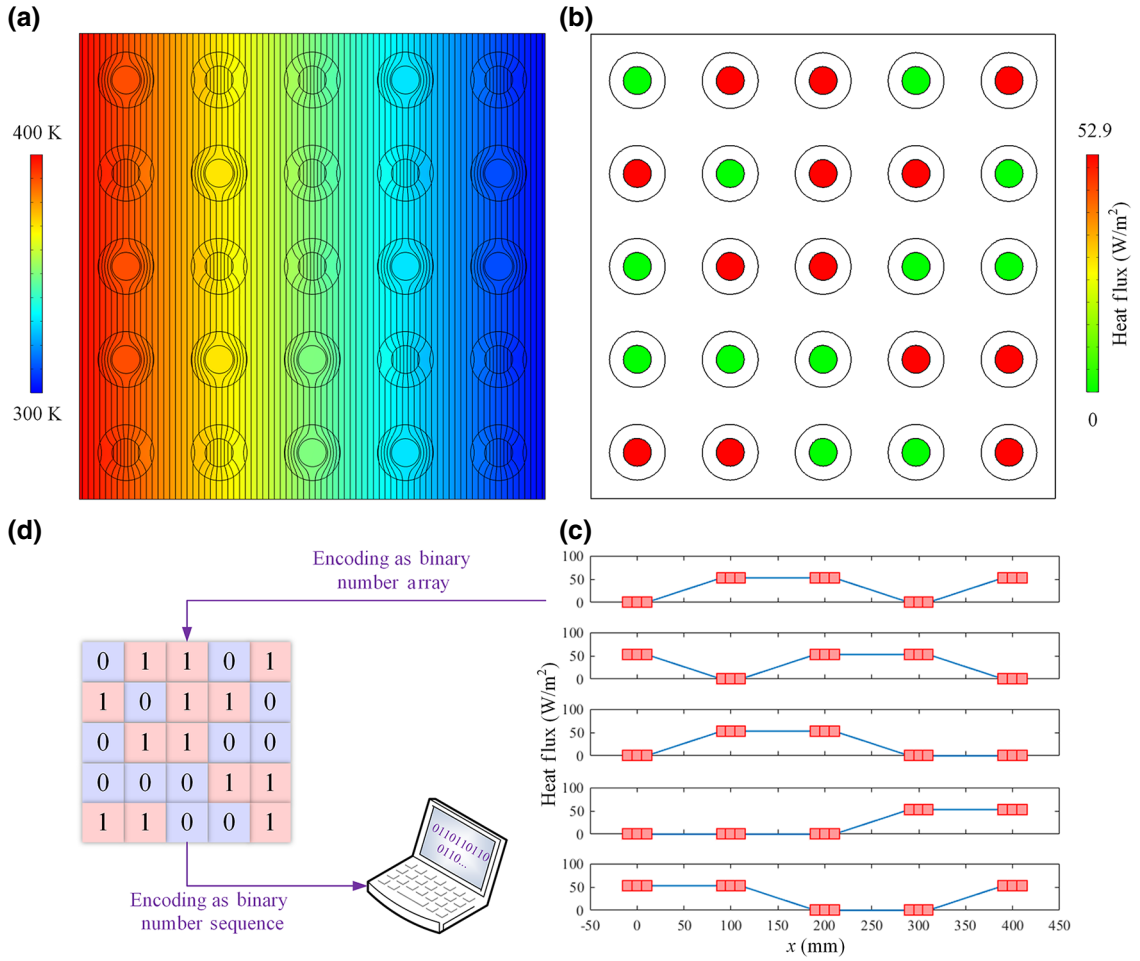

FIG. 4. Two-dimensional thermal encoding based on an array of ESUs and EHUs. (a) Steady temperature profile and isotherms of a 5×5 ESUs and EHUs array. The dimensions of the whole plane 500×500 mm^2, while each ESU and EHU has the same dimension as those in Fig. 1. All the other simulation conditions are the same. (b) Local heat flux in the inner cylinders in the ESU and EHU array. (c) Heat flux curves detected by all of the probes. Based on such an encoding protocol, the ESUs and EHUs in (a) can be encoded as the array of binary numbers in (d). The binary number array can be stored in a computer either along the column direction or along the row direction.

thermocouple. The distance between the copper plate and the IR camera is approximately 0.7 m, and we fine tune the camera to make the image clear. The simulated and experimental temperature fields are shown in Figs. 5(c) and 5(d), and agree with each other well. It is seen in Fig. 5(c) that there are isotherms in the inner cylinders in the EHUs, while there are no isotherms in the ESUs, which indicates that the heat is shielded by the ESUs and harvested by the EHUs. Nearly no heat enters the inner cylinders of the ESUs and more heat enters the inner cylinders of the EHUs, resulting in completely different local heat-flux levels. The local heat fluxes in the inner cylinders are calculated according to Fourier's law $q = -\kappa dT/dx \approx -\kappa \Delta T/\Delta x$. For a better comparison of the simulated and experimental local heat fluxes, we define a nondimensional heat flux as $q^* = q/q_{\max}$. These are plotted in Figs. 5(e) and 5(f), respectively. Both in the simulation and in the experiment, we find that $q^*_{\mathrm{EHU}} > q^*_{\mathrm{RU}} > q^*_{\mathrm{ESU}}$, which verifies the energy shielding/harvesting effects correspond to the isothermal contours in Fig. 5(c). As for the encoding process, we can define a critical heat flux level q^*_{cr}. If setting $q^*_{\mathrm{EHU}} > q^*_{\mathrm{cr}} > q^*_{\mathrm{RU}} > q^*_{\mathrm{ESU}}$, then the experimental demonstration can be encoded as 0100-0100; if setting $q^*_{\mathrm{EHU}} > q^*_{\mathrm{RU}} > q^*_{\mathrm{cr}} > q^*_{\mathrm{ESU}}$, then the experimental demonstration can be encoded as 1100-0111. The reason that we introduce the reference unit into the experiment rather than into the previous demonstration is to show the encryption capability of the proposed thermal encoding concept. The encoded binary information can be encrypted depending on our preset communication protocol. Although the present simulations and experiments are in the macroscale regime, such encoding concepts can also be extended to micro/nanoscale phonon transport for the microminiaturization of the encoding device development.

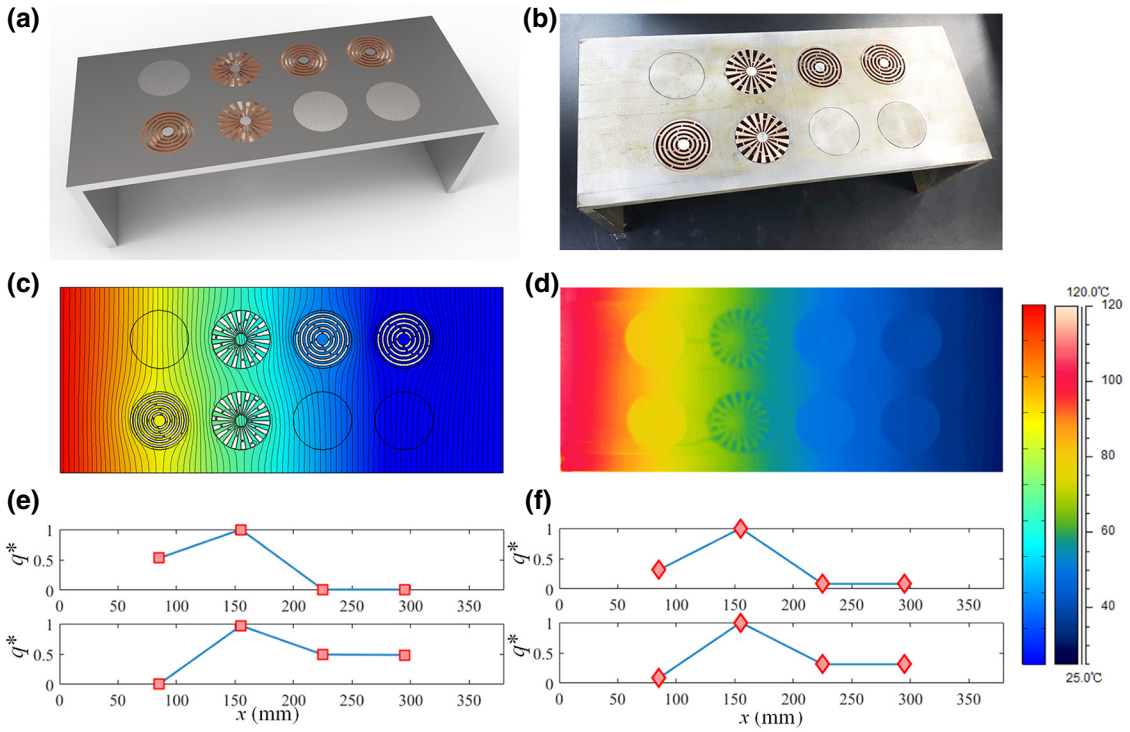

FIG. 5. (a) Schematic and (b) prototype of an experimental demonstration of binary thermal encoding. (c) Simulated and (d) experimental temperature fields of the prototype. Heat flux across the inner cylinders of each unit in (e) simulation and (f) experiment.

The proposed thermal encoding based on the ESUs and EHUs is inspired by the binary states of the heat fluxes in such two thermal structures. The heat flux in ESU is almost zero while the heat flux in EHU is stable at a certain value. Both are independent of the local temperature. The underlying physics behind such two different consequences can be attributed to the required transformed thermal conductivity tensors of ESU and EHU. The present ESUs and EHUs are in the cylindrical coordinates, thus the demonstrated thermal encoding is based on 1D and 2D distributions of the ESU and EHU, but it is easy to perceive that such a thermal encoding scheme can also be extended to 3D when changing the cylindrical coordinates to spherical coordinates. The heat fluxes in a 3D spherical ESU and EHU matrix should be at two different states as well, and can be interpreted and encoded as binary numbers in a 3D matrix. As for the real implementation, such a thermal encoding is similar to movable-type typography, and the ESU and EHU can be assembled at the desired locations to exhibit binary heat flux states depending on the desired encoding number.

IV. CONCLUSIONS

In summary, we propose a different kind of thermal encoding protocol based on the ESUs and EHUs by taking advantage of the different two states of heat fluxes in the central regions. The two states of the heat fluxes in the ESUs and EHUs are demonstrated by transformation thermotics, and explained by the anisotropic distribution of the transformed thermal-conductivity tensor. A mathematical model is developed to show the upper and lower bounds of heat fluxes for ESU and EHU for better understanding of the binary states. Based on the ESU and EHU, 1D and 2D thermal encodings are demonstrated and can also be extended to 3D thermal encoding. Transient analyses of the ESU and EHU behaviors reveal that the proposed thermal encoding can be applied even in the transient scheme without waiting for a slowly developing temperature equilibrium state. Experiments further reveal that such thermal encoding can be encrypted dependent on a preset critical heat flux and the communication protocol. Such a type of thermal encoding is similar to the movable-type typography. The ESU and EHU act as movable modules and can be assembled at desired locations to exhibit two heat flux states depending on the desired encoding number. Such a thermal encoding may be applied for further development of thermal memory and thermal computing, and open an additional avenue for triggering counterpart developments in other physical fields, such as optical, electromagnetic, acoustic, etc.

ACKNOWLEDGMENTS

The authors would like to acknowledge the financial support by National Natural Science Foundation of China

(Grants No. 51606074 and No. 51625601), the Ministry of Science and Technology of the People's Republic of China (Grant No. 2017YFE0100600), and the National Key R&D Program of China (Grant No. 2016YFB0400804).

[1] C. Z. Fan, Y. Gao, and J. P. Huang, Shaped graded materials with an apparent negative thermal conductivity, Appl. Phys. Lett. **92**, 251907 (2008).
[2] J. B. Pendry, D. Schurig, and D. R. Smith, Controlling electromagnetic fields, Science **312**, 1780 (2006).
[3] U. Leonhardt, Optical conformal mapping, Science **312**, 1777 (2006).
[4] X. Y. Shen, Y. Li, C. R. Jiang, and J. P. Huang, Temperature Trapping: Energy-Free Maintenance of Constant Temperatures as Ambient Temperature Gradients Change, Phys. Rev. Lett. **117**, 055501 (2016).
[5] Y. Li, X. Y. Shen, Z. H. Wu, J. Y. Huang, Y. X. Chen, Y. S. Ni, and J. P. Huang, Temperature-Dependent Transformation Thermotics: From Switchable Thermal Cloaks to Macroscopic Thermal Diodes, Phys. Rev. Lett. **115**, 195503 (2015).
[6] T. Han, T. Yuan, B. Li, and C.-W. Qiu, Homogenous thermal cloak with constant conductivity and tunable heat localization, Sci. Rep. **3**, 1593 (2013).
[7] S. Guenneau, C. Amra, and D. Veynante, Transformation thermodynamics: Cloaking and concentrating heat flux, Opt. Express **20**, 8207 (2012).
[8] S. Narayana and Y. Sato, Heat Flux Manipulation with Engineered Thermal Materials, Phys. Rev. Lett. **108**, 214303 (2012).
[9] R. Hu, S. L. Zhou, X. J. Yu, and X. B. Luo, Exploring the proper experimental conditions in 2D thermal cloaking demonstration, J. Phys. D: Appl. Phys. **49**, 415302 (2016).
[10] R. Hu, X. L. Wei, J. Y. Hu, and X. B. Luo, Local heating realization by reverse thermal cloak, Sci. Rep. **4**, 3600 (2014).
[11] T. Han, J. Zhao, T. Yuan, D. Y. Lei, B. Li, and C. W. Qiu, Theoretical realization of an ultra-efficient thermal-energy harvesting cell made of natural materials, Energy Environ. Sci. **6**, 3537 (2013).
[12] F. Chen and D. Y. Lei, Experimental realization of extreme heat flux concentration with easy-to-make thermal metamaterials, Sci. Rep. **5**, 11552 (2015).
[13] S. Guenneau and C. Amra, Anisotropic conductivity rotates heat fluxes in transient regimes, Opt. Express **21**, 6578 (2013).
[14] R. Hu, B. Xie, J. Y. Hu, Q. Chen, and X. B. Luo, Carpet thermal cloak realization based on the refraction law of heat flux, Europhys. Lett. **111**, 54003 (2015).
[15] R. Hu, S. L. Zhou, W. C. Shu, B. Xie, Y. P. Ma, and X. B. Luo, Directional heat transport through thermal reflection meta-device, AIP Adv. **6**, 125111 (2016).
[16] R. Hu, S. L. Zhou, Y. Li, D. Y. Lei, X. B. Luo, and C. W. Qiu, Illusion thermotics, Adv. Mater. **30**, 1707237 (2018).
[17] S. L. Zhou, R. Hu, and X. B. Luo, Thermal illusion with twinborn-like heat signatures, Int. J. Heat Mass Transf. **127**, 607 (2018).
[18] X. Shen, Y. Li, C. Jiang, Y. Ni, and J. P. Huang, Thermal cloak-concentrator, Appl. Phys. Lett. **109**, 031907 (2016).
[19] G. Atwood, Phase-change materials for electronic memories, Science **321**, 210 (2008).
[20] M. Mannini, F. Pineider, P. Sainctavit, C. Danieli, *et al.*, Magnetic memory of a single-molecule quantum magnet wired to a gold surface, Nat. Mater. **8**, 194 (2009).
[21] F. Xiong, A. D. Liao, D. Estrada, and E. Pop, Low-power switching of phase-change materials with carbon nanotube electrodes, Science **332**, 568 (2011).
[22] R. Simpson, E. P. Fons, A. V. Kolobov, T. Fukaya, M. Krbal, T. Yagi, and J. Tominaga, Interfacial phase-change memory, Nat. Nanotechnol. **6**, 501 (2011).
[23] E. Kuramochi and M. Notomi, Phase-change memory, Nat. Photonics **9**, 712 (2015).
[24] L. Wang and B. Li, Thermal Memory: A Storage of Phononic Information, Phys. Rev. Lett. **101**, 267203 (2008).
[25] N. Li, J. Ren, L. Wang, G. Zhang, P. Hanggi, and B. Li, Colloquium: Phononics: Manipulating heat flow with electronic analogs and beyond, Rev. Mod. Phys. **84**, 1045 (2012).
[26] R. Xie, C. T. Bui, B. Varghese, O. Zhang, C. H. Sow, B. Li, and J. T. L. Thong, An electrically tuned solid state thermal memory based on metal-insulator transition of single-crystalline VO_2 nanobeams, Adv. Funct. Mater. **21**, 1602 (2011).
[27] X. Sun, B. Yu, and M. Meyyappan, Synthesis and nanoscale thermal encoding of phase-change nanowires, Appl. Phys. Lett. **90**, 183116 (2007).